A Realistic Multiregion Mouse Kidney Dosimetry Model to Support the Preclinical Evaluation of Potential Nephrotoxicity of Radiopharmaceutical Therapy

Clarita Saldarriaga Vargas[1,2], Lara Struelens[1], Matthias D'Huyvetter[2], Vicky Caveliers[2], and Peter Covens[2]

[1]Radiation Protection Dosimetry and Calibrations, Belgian Nuclear Research Centre (SCK CEN), Mol, Belgium; and [2]Department of Medical Imaging, Laboratory for In Vivo Cellular and Molecular Imaging, Vrije Universiteit Brussel, Brussels, Belgium

Suborgan absorbed dose estimates in mouse kidneys are crucial to support preclinical nephrotoxicity analyses of α- and β-particle–emitting radioligands exhibiting a heterogeneous activity distribution in the kidneys. This is, however, limited by the scarcity of reference dose factors (S values) available in the literature for specific mouse kidney tissues. **Methods:** A computational multiregion model of a mouse kidney based on high-resolution MRI data from a healthy mouse kidney was developed. The model was used to calculate S values for 5 kidney tissues (cortex, outer and inner stripes of outer medulla, inner medulla, and papilla and pelvis) for a wide range of β- or α-emitting radionuclides (45 in total) of interest for radiopharmaceutical therapy, using Monte Carlo calculations. Additionally, regional S values were applied for a ^{131}I-labeled single-domain antibody fragment with predominant retention in the outer stripe of the renal outer medulla. **Results:** The heterogeneous activity distribution in kidneys of considered α- and low- to medium-energy β-emitters considerably affected the absorbed dose estimation in specific suborgan regions. The suborgan tissue doses resulting from the nonuniform distribution of the ^{131}I-labeled antibody fragment largely deviated (from -40% to 57%) from the mean kidney dose resulting from an assumed uniform activity distribution throughout the whole kidney. The absorbed dose in the renal outer stripe was about 2.0 times higher than in the cortex and in the inner stripe and about 2.6 times higher than in inner tissues. **Conclusion:** The use of kidney regional S values allows a more realistic estimation of the absorbed dose in different renal tissues from therapeutic radioligands with a heterogeneous uptake in the kidneys. This constitutes an improvement from the simplistic (less accurate) renal dose estimates assuming a uniform distribution of activity throughout kidney tissues. Such improvement in dosimetry is expected to support preclinical studies essential for a better understanding of nephrotoxicity in humans. The dosimetric database has added value in the development of new molecular vectors for radiopharmaceutical therapy.

Key Words: multiregion mouse kidney model; suborgan dosimetry; radiopharmaceutical therapy; MIRD; autoradiography

In radiopharmaceutical therapy, the transit and temporary retention of radioligand in the kidneys during renal elimination result in a local irradiation of kidney tissues that can cause absorbed dose–limiting nephrotoxicity. Consequently, nephrotoxicity is often the focus of absorbed dose escalation studies on mice during the preclinical testing of novel radioligands and the preclinical investigation of treatment optimization strategies beyond radioligand design. Additionally, the distribution of a radioligand is often not uniform in the kidney (*1–3*). Small, fast-clearing radiopharmaceuticals often show increased retention in the proximal tubules of the renal cortex and (or) in the outer stripe of the renal outer medulla (OSOM) (Fig. 1) (*2,4,5*). This increase can lead to a corresponding nonuniform distribution of absorbed dose and tissue damage across renal regions (*1,6*) and even in specific substructures within them (*7*), particularly for radionuclides emitting charged-particle radiation with a limited penetration range in tissue, such as α-particles and low- to medium-energy electrons and β-particles.

Accurate dosimetry of specific mouse kidney tissues is essential for interpreting the outcomes of preclinical nephrotoxicity studies. Understanding the impact in nephrotoxicity of the local tissue damage resulting from the nonuniform dose distribution of radiopharmaceuticals is of increased importance in kidney tissues, which have a complex functional architecture and potentially differ in radiobiologic response (*8*). An aspect that precludes a more realistic kidney-tissue dosimetry of heterogeneous radioligand distributions is the scarcity of reference radionuclide S values (factors of absorbed dose per radionuclide decay) for relevant tissue regions of the mouse kidney. S values are dependent on the radionuclide radiation emissions and the geometry of the anatomic model used for modeling the radiation source and for absorbed dose calculations. Some dosimetry models of murine kidneys exist that allow an accounting, to some extent, for nonuniform distributions of radionuclides (*1,5,6*). Their application in preclinical studies is, however, limited by the few compartments used to represent the renal structure and consequently the heterogeneity of the organ activity distribution. Furthermore, S values are available for only a limited number of radionuclides.

The aim of this work was to develop a computational realistic multiregion model of a mouse kidney, based on high-resolution MRI data, to facilitate suborgan kidney dosimetry in preclinical investigations of radiopharmaceutical therapy. Next, the model was used to calculate suborgan regional S values for the kidney for a wide range of radionuclides of interest in radiopharmaceutical therapy. Finally, suborgan kidney dosimetry was demonstrated for a ^{131}I-radiolabeled single-domain antibody fragment (sdAb) that has predominant retention in the outer stripe of the renal outer medulla and is currently being evaluated clinically for radiopharmaceutical therapy of cancer expressing the human epidermal growth factor receptor type 2 (*9*).
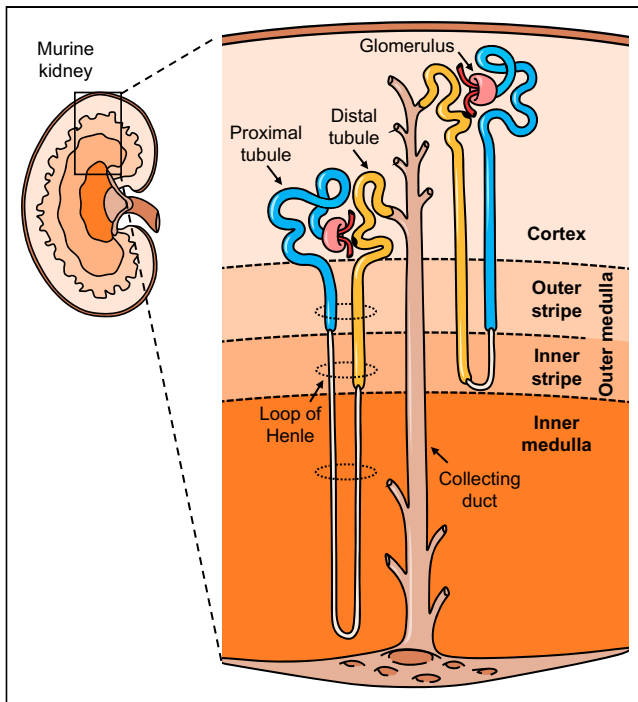
FIGURE 1. Microscopic anatomy of kidney tissues. Main nephron parts and different kidney regions to which they belong are indicated.

MATERIALS AND METHODS

A condensed version of the materials and methods is given here. The complete version can be found in the online supplemental data (supplemental materials are available at http://jnm.snmjournals.org).

All animal experiments were conducted in accordance with the guidelines, and after the approval, of the Ethical Committee of the Vrije Universiteit Brussel.

Development of Kidney Model

A schematic overview of the main steps involved in the development of the 3-dimensional (3D) kidney model is shown in Figure 2.

The kidney model was developed using as a reference high-resolution (43 × 78 × 78 μm voxels) MRI data obtained ex vivo on a perfusion-fixed kidney excised from a healthy mouse (C57BL/6, female, 9 wk old, 19.5-g body weight). MRI was performed with a horizontal 7-T preclinical scanner (PharmaScan; Bruker BioSpin).
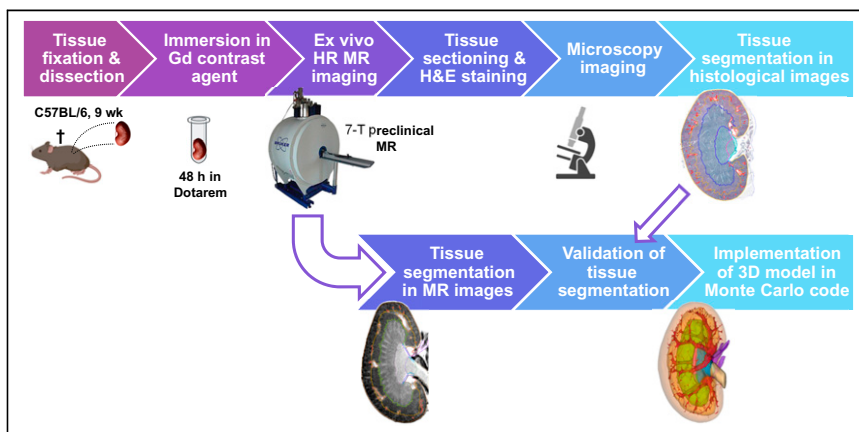

FIGURE 2. Workflow diagram of development of multiregion kidney model. H&E = hematoxylin and eosin; HR = high resolution.

Ten volume regions were segmented on the MR image using 3D-Slicer software (http://www.slicer.org). The segmented regions corresponded to 4 tissues of the renal parenchyma (the renal cortex including its vasculature [C], the OSOM including its vasculature [OS], the inner stripe of the outer medulla [IS], and the inner medulla including some vasculature [IM]), the main arteries and veins within the renal parenchyma, the renal papilla, the renal pelvis, part of the external renal vessels, part of the ureter, and uniform surrounding tissue. The kidney model was created by merging all the segmented regions into a single 3D matrix consisting of $127 \times 62 \times 125$ (~1 million) voxels, with same voxel dimensions as the MR dataset.

Tissue segmentation was validated against regions of interest drawn on conventional histology images of the same kidney.

Calculation of S Values and Absorbed Energy Fractions

The $S(r_T \leftarrow r_S)$ values (where r_S is source region and r_T is target region) and absorbed energy fractions of different kidney tissues were calculated for the kidney model using Monte Carlo radiation transport simulations with MCNP, version 6.2 (Los Alamos National Laboratory).

Monte Carlo calculations were performed for 12 β-emitting radionuclides (^{32}P, ^{47}Sc, ^{67}Cu, ^{89}Sr, ^{90}Y, ^{131}I, ^{153}Sm, ^{161}Tb, ^{166}Ho, ^{177}Lu, ^{186}Re, and ^{188}Re) and for the α-emitters shown in Supplemental Figure 1 (decay schemes for ^{225}Ac, ^{227}Th, ^{230}U, ^{224}Ra, ^{211}At, and ^{149}Tb) and their progeny, which includes α-, β-, or positron emitters. Radionuclide radiation emission data from International Commission on Radiological Protection report 107 (10) were used for modeling the radiation sources. Absorbed energy fractions for self-irradiation were calculated for monoenergetic electrons (20–2,500 keV), α-particles (3–10 MeV), and photons (10–1,500 keV).

r_S and r_T for S value and absorbed energy fraction calculations include C, OS, IS, IM, and renal papilla and pelvis (PP). These regions, all together, represent the whole kidney region (K), which was used also as an r_S and r_T in the case of a uniform activity distribution throughout kidney tissues. For each radionuclide, the activity was uniformly distributed in each r_S and the absorbed dose per decay was simulated.

Kidney Dosimetry Study

A dosimetry study was performed to demonstrate use of the S values calculated with the kidney model. The radioligand used to derive the mouse kidney biodistribution was the iodinated sdAb 2Rs15d (^{131}I-sdAb) (11).

Healthy mice ($n = 5$; C57BL/6; female; 9 wk old; mean body weight $\pm$ SD, 20.7 ± 1.0 g) were anesthetized by inhalation with 2% isoflurane and were injected in the tail vein with 13.0 ± 3.3 MBq of ^{131}I-sdAb (5 μg of sdAb). At 1, 3, 6, 24, and 70 h after injection, mice ($n = 1$ per time point) were euthanized by cervical dislocation. The kidneys were dissected and weighed, and their activity was measured in a γ-counter using an optimized measurement protocol (12). The fraction of injected activity per gram of dissected kidney tissue was calculated.

The suborgan distribution of ^{131}I-sdAb in kidney tissues was determined with high-resolution quantitative digital autoradiography using an ionizing-radiation quantum imaging detector (13). Each autoradiography image was quantified in ImageJ–Fiji (https://imagej.net/software/fiji/) using detailed regions of interest drawn on histologic images of the same section as used for autoradiography or an adjacent kidney section. A region of interest was drawn on each of the 5 tissues considered as r_S in the kidney model (C, OS, IS, IM, and PP), and the mean of the counts per minute of the region-of-interest pixels was estimated.

Suborgan regional dosimetry for kidney tissues was performed following the MIRD methodology. Two source distributions were considered: the first was a time-dependent nonuniform activity distribution based on the relative autoradiography data, and the second was a simplified case in which activity was assumed to be uniformly distributed throughout kidney tissues (i.e., $r_S = r_T = K$).

For each time point, the absorbed dose rate in each r_T delivered by the activities measured in each r_S of the kidney model was based on the S values calculated for the proposed kidney model. The activity of the whole kidney was determined with γ-counting, and the relative suborgan distribution of activity was measured with autoradiography (for the first type of source distribution only).

Absorbed dose rates as a function of time were analyzed by nonlinear least-squares fitting (MATLAB; MathWorks) to a negative power function of time after injection. For each of the 2 source distributions considered, the absorbed dose per unit of injected activity ($D(r_T)/A_0$, where D is absorbed dose and A_0 is injected activity decay corrected to the mouse time of death) was estimated for each r_T, applying mathematic integration of dose rate values from the time of injection (time = 0) to infinity.

RESULTS

Kidney Model

There was good agreement between the histology-based tissue regions of interest and the MR-based regions of interest used to define the kidney model (Fig. 3A, with additional comments in the supplemental data).

FIGURE 3. (A) Validation of MR-based kidney-tissue segmentation against histology. (B and C) Kidney model 3D rendering with transparency view (B) and coronal (left) and transverse (bottom right) cross-section views (C) of kidney lattice as implemented in Monte Carlo code. ISOM = inner stripe of the renal outer medulla.

The main orthogonal dimensions of the kidney model are around $5.3 \times 4.6 \times 9.5$ mm (excluding ureter and external vessels). In mouse kidneys, unlike human kidneys, medullary tissues are not organized into multiple pyramids and form instead a single bean-shaped body (Fig. 3) (14). As such, there are no renal calyces, and a single renal papilla connects directly and deeply with the renal pelvis. The cortex and the OSOM tissues appear as adjacent rims (each with a thickness of ~0.6 mm) surrounding most of the inner tissues. The masses and percentage volume occupancy of each tissue region are listed in Table 1. The 3D dataset of the kidney model can be found in the supplemental file "Kidney_model_dataset.nii."

S Values

S values for the considered α- and β-emitting radionuclides are listed in Supplemental Tables 1–3. The simulation statistical error of all the reported S values was within 3%, unless otherwise specified. A subset of the S values is graphically shown in Figure 4 for a selection of β- and α-emitters (and their progeny). The absorbed energy fractions for electrons, α-particles, and photons are shown in Supplemental Figure 2.

High-energy β-emitters (e.g., ^{90}Y, ^{188}R, and ^{32}P) typically result in higher S values and more cross-irradiation between the source tissue and surrounding tissues than low-energy β-emitters (e.g., ^{177}Lu, ^{67}Cu, ^{161}Tb, and ^{131}I). Cross-irradiation is nevertheless substantial also for low-energy β-emitters, particularly between adjacent target–source kidney tissue regions (e.g., C←OS and IS←OS). The S values for self-irradiation (e.g., C←C and OS←OS) are somewhat higher for radionuclides with an abundant yield of Auger and internal-conversion electrons (^{161}Tb, ^{153}Sm, and ^{166}Ho), as these typically low-energy electrons are absorbed more locally than the more energetic β- particles (Supplemental Figs. 2 and 3).

The energy emitted by α-emitters is absorbed mostly within the r_S itself, and cross-irradiation is small between adjacent tissues and negligible between more distant tissues (e.g., IS←C and IM←OS). Indeed, the absorbed fractions for self-irradiation with α-particles are mostly 0.90 or more for most tissue regions (Supplemental Fig. 2).

Kidney Dosimetry Study

The pharmacokinetics of ^{131}I-sdAb in mouse kidney tissues are fast. Kidney uptake at 24 h after ^{131}I-sdAb administration is less than 0.5% of that at 1 h after injection (Supplemental Table 4). The autoradiography images (Fig. 5) clearly indicate a nonuniform and time-dependent biodistribution. During the first 24 h after radioligand administration, retention is prominent in the OSOM tissue and then in the cortex tissue (Supplemental Table 4). This observation is likely due to a partial reabsorption of the ^{131}I-sdAb in the proximal tubules located exclusively in these 2 tissues, and particularly in the straight segments that densely
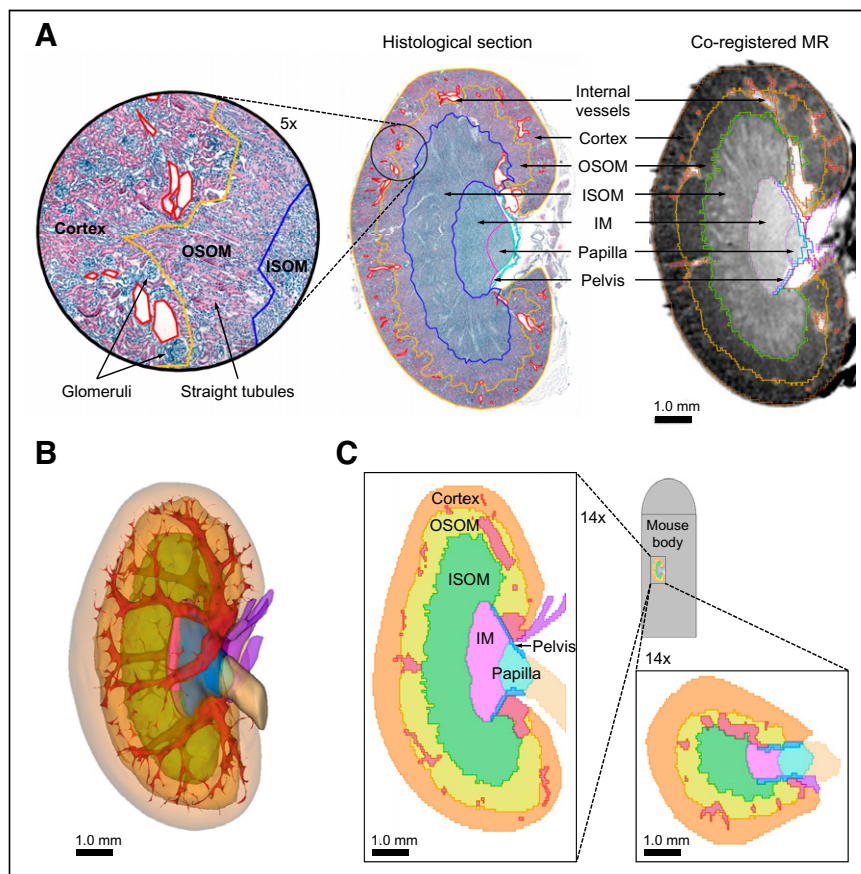
TABLE 1
Mass and Percentage Volume Occupancy of Kidney Model Regions Used as r_S or r_T, Including Blood Vessels

r_T or r_S	Mass (mg)		Volume, region (%)
	Region	Vessels	
C	60.2	1.4	51
OS	37.3	3.5	32
IS	16.4	0.4	14
IM	2.0	—	2
PP	1.5	—	1
K	117.5	5.3	100

occupy the OSOM (Fig. 1). From 24 h after injection onward, the little activity that remains in the kidney is more concentrated in the cortex tissue, although the nonuniformity across tissues is less pronounced than at earlier time points. The concentration of activity in the inner tissues (ISOM, papilla and pelvis) is always lower than in the renal cortex and the OSOM tissues.

The distribution of ^{131}I-sdAb activity in kidney tissues has a substantial impact on estimation of time-dependent absorbed dose rates (Fig. 6B) and absorbed doses (Table 2), per unit of injected activity, in specific kidney tissues. Compared with the more realistic nonuniform source distribution, the assumption of a uniform distribution of activity throughout the kidney tissues ($r_S = r_T = K$) results in a strong underestimation of the absorbed dose rate in the OSOM and an overestimation of the absorbed dose rate in the other tissues (including the renal cortex) at early time points (<24 h after injection). A similar effect

results in the absorbed doses, because for ^{131}I-sdAb the high activities at early time points dominate the estimation of the time-integrated absorbed dose. The absorbed dose is about 2.0 times higher in the OSOM than in the renal cortex and the ISOM tissues, and about 2.6 times higher than in inner tissues.

DISCUSSION

The calculated regional S values indicate that consideration of the heterogeneity in activity distribution in mouse kidneys can have a considerable impact on the absorbed dose estimations of specific tissues, particularly for radionuclides that emit α-particles and low- to medium-energy β-particles. This was demonstrated for the nonuniform mouse kidney biodistribution of a ^{131}I-labeled sdAb that is predominantly and temporarily retained in the OSOM. ^{131}I emits low- to medium-energy β-particles (182 keV on average) with a short penetration range in tissue (~0.4 mm on average) when compared with the size of mouse kidney tissues. Therefore, self-irradiation is the main contributor (~87%) to the absorbed dose rates in the OSOM at early time points (Supplemental Fig. 4). This holds true also for the renal cortex (~71% from self-irradiation), although with an also-important contribution (~29%) of cross-irradiation from activity in the OSOM. This leads to a substantially nonuniform absorbed dose distribution across different kidney tissues in which the OSOM is the most irradiated tissue.

This study presented a realistic 3D model of mouse kidney tissues useful for preclinical internal radiation dosimetry. The regional S values calculated with the proposed model allow a more detailed and realistic estimation of absorbed doses in different renal tissues from β- and α-emitters, accounting for the heterogeneous activity distribution. Exploitation of the full potential of the proposed model would require information on the suborgan activity distribution at the regional-tissue level as a function of time. Such information can be derived from ex vivo mouse biodistribution studies using quantitative high-resolution autoradiography of β- or α-particles of tissue sections of mice killed at different sampling time points, complemented by γ-counting of the whole kidney to measure kidney activity, as demonstrated in this study. Alternatively, quantitative emission tomography imaging can be used to measure kidney activity thoroughly over time and in vivo (12), which would enable longitudinal studies (such as nephrotoxicity studies) on the same mice as are used for organ-level pharmacokinetic assessment. In such a case, autoradiography measurements may be performed on separate mice at selected time points of the pharmacokinetic profile, chosen, for example, to sample regions of high activity or when the subkidney distribution is more likely to vary (absorption, distribution, elimination phases). The mouse kidney model may be seen as an analog of the model of a human kidney presented in MIRD pamphlet 19 (3), with some differences being that the former is used for preclinical dosimetry of mouse tissues and provides a more realistic representation of kidney tissues, which additionally considers the OSOM as a separate source/target compartment. Modeling of OSOM tissues is
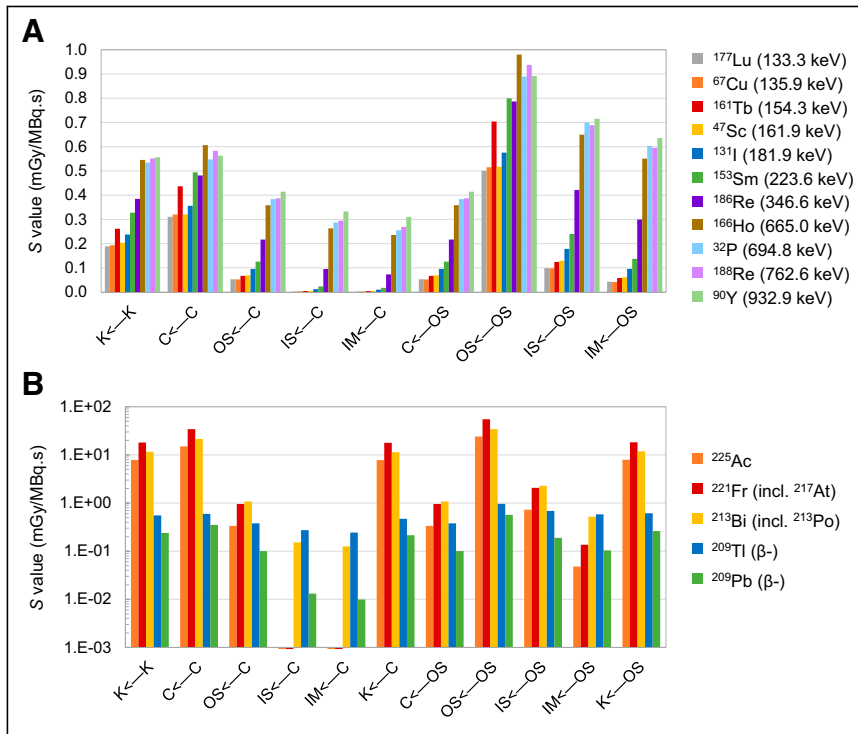
FIGURE 4. S values for some β-emitters (A) and for ^{225}Ac and some of its progeny (B), for selected source and target tissues. For convenience, radionuclide series in A are listed in order of increasing mean β-particle energy per β-decay (values in parentheses in series legends).
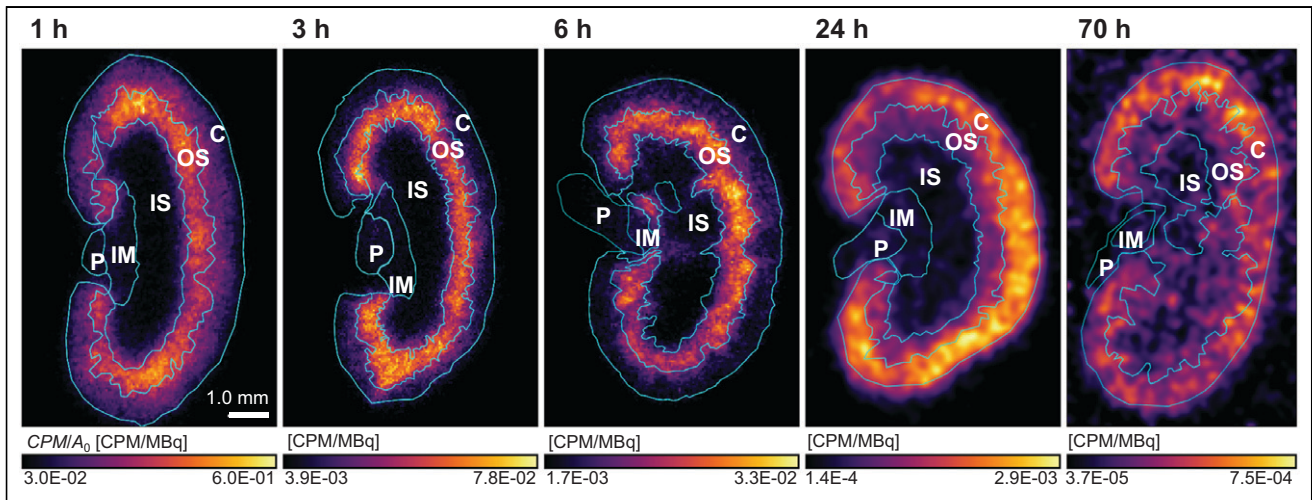
FIGURE 5. Autoradiography images of kidney tissues of mice killed at 1, 3, 6, 24 and 70 h after injection of ^{131}I-sdAb. Autoradiography data at 24 and 70 h after injection were smoothed with 2.0-σ gaussian filter for visualization only. Regions of interest used for quantification are shown in cyan. CPM = counts per minute; CPM/A_0 = counts per minute per injected activity decay corrected to the mouse time of death.

pertinent for dosimetry in view of the possible substantial radioligand retention in the straight segments of the proximal tubules, which physically extend from the renal cortex to the OSOM in both humans and rodents. The early biodistribution of ^{131}I-sdAb considered here for the dosimetry study is a good example of such a situation.

For α-particle emitters, subregional dosimetry at the level of mouse nephron substructures (e.g., glomerulus and specific segments of the tubule) can be of interest. Although miniaturized versions of models of a human nephron can be used for that purpose (7), their use in preclinical investigation of radiopharmaceuticals is limited by the difficulty in determining the distribution of radionuclide activity at the level of nephron substructures. The intermediate (i.e., regional) dosimetry of α-particle emitters achievable with the regional S values presented here might be useful when suborgan activity information is available at only a more regional (tissue) level.

S factors are sensitive to the target tissue mass and to the absorbed energy fraction, which is sensitive to the target–source geometry. Besides, the size of kidney tissues may vary with mouse strain, age, health condition, and other factors. Therefore, inaccuracies in absorbed dose estimations might arise from anatomic differences between the

kidney model and the kidneys of mice used in preclinical studies. Mass scaling of the regional S values to the actual (measured) mass of the kidney (factor $M_K/\bar{M}_{kidney}$ in Supplemental Eq. 1) can compensate for the effect of the r_T mass in the absorbed dose estimations, assuming that the occupancy volumes of the measured tissues is the same as in Table 1. However, mass scaling does not account for deviations in the absorbed energy fractions due to, for example, differences in the thickness of the C rim or of the OS rim associated with tissues with sizes or volumes of occupancy different from the kidney model. The impact of these factors may be investigated using simplified models (such as those based on ellipsoidal shells to represent tissue compartments (6)), and if relevant, correction factors may be determined to be applied to absorbed dose estimations with the regional S values reported here. Such analyses were beyond the scope of this study.

Svensson et al. used a stylized 3-region, 0.15-g kidney model based on spheroids to calculate regional absorbed energy fractions for ^{177}Lu and [90]Y β-particles emitted by the renal cortex (5). Compared with that model, the ^{177}Lu and [90]Y β-particle absorbed fractions calculated with the more realistic model proposed in this study are, respectively, 6% and 19% lower for self-irradiation of the C (absorbed energy fraction, 0.79 for ^{177}Lu and 0.23 for ^{90}Y) and 62% and 36% higher for cross-irradiation between the renal cortex and the OSOM (absorbed energy fraction, 0.082 for ^{177}Lu and 0.10 for ^{90}Y). These dosimetric discrepancies are likely related to differences in geometry and size of kidney tissue regions between the 2 models.

More realistic absorbed dose estimates of mouse kidney tissues can support the analysis of preclinical nephrotoxicity studies of therapeutic radioligands, such as the investigation of absorbed dose thresholds for toxicity of specific kidney tissues (or substructures) resulting from nonuniform irradiations with radionuclides (5,6,8). Such insight can be relevant for the design of first-in-humans trials with novel radioligands,
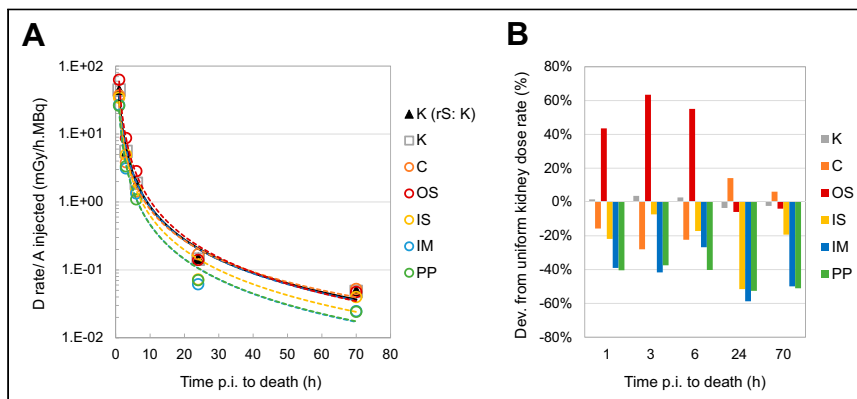

FIGURE 6. (A) Dose rates per unit of injected activity in different tissue regions and in K, as function of time after injection of ^{131}I-sdAb, for heterogeneous activity distribution based on autoradiography data (Supplemental Table 4) and for assumed uniform activity distribution throughout kidney (r_S = K). Curves indicate power function fit of each r_T (Supplemental Table 5). (B) Percentage deviations from uniform dose rate throughout kidney tissues (r_S = K). A = activity; D = absorbed dose; p.i. = after injection.

TABLE 2
Absorbed Doses Delivered to Different Tissue Regions and to K per Unit of Injected Activity Decay Corrected to the Mouse Time of Death, for Heterogeneous Activity Distribution Based on Autoradiography Data* and for Assumed Uniform Activity Distribution Throughout K

| Parameter | Heterogeneous activity distribution | | | | | | Uniform activity $(r_S = K)$, K |
	K	C	OS	IS	IM	PP	
Absorbed dose per injected activity, $D(r_T)/A_0$ (mGy·MBq^{-1})	73.1	54.8	111.6	62.3	43.0	43.6	71.2
Deviation from $D(r_T = r_S = K)/A_0$ (%)	3	−23	57	−12	−40	−39	—

*Supplemental Table 4.

by informing about potential toxicities due to the predicted absorbed dose distribution in larger kidney tissues such as in humans. The glomeruli are sometimes thought to be the absorbed dose–limiting renal substructures when dealing with β-radiotherapeutics (8,15). Yet, loss of proximal tubules has also been associated with long-term nephrotoxicity in mice with either β- or α-emitting radioligands (5,16). Investigating the absorbed dose dependence of glomerular and proximal tubular damage is therefore of high interest and would benefit from more detailed dosimetry at the level of suborgan regions or even at the level of nephron substructures. Additionally, translational and back-translational research on the renal absorbed dose–toxicity relationships might support the investigation of treatment optimization strategies beyond radioligand design, such as renoprotective agents that reduce reabsorption and internalization by the proximal tubule cells (4,5) and activity fractionation (8,15).

An improved understanding of radiation-induced nephrotoxicity in the presence of absorbed dose (and dose-rate) heterogeneity after radiopharmaceutical therapy should improve the implementation of optimized and patient-specific procedures (8). In peptide receptor radionuclide therapy, for example, the microscopic absorbed dose distribution in human kidneys is thought to play a role in the seemingly lower incidence of nephrotoxicity of ^{177}Lu-labeled somatostatin analogs than of similar ^{90}Y-labeled peptides (2,17). Clinical investigation of the influence of absorbed dose nonuniformity on nephrotoxicity is, however, a challenge, as it would require the availability of a large amount of good-quality patient-specific detailed dosimetry and response data on the kidneys for each therapeutic setting (18). Conversely, animal experiments allow determination of the microscopic distribution of radiopharmaceuticals in tissues ex vivo and investigation of the biologic response associated with radiopharmaceutical therapy in a more reproducible and controlled experimental setting. The S values for regions of the mouse kidney presented here could facilitate preclinical absorbed dose estimations required to investigate the contribution to nephrotoxicity of the absorbed dose-dependent damage to different kidney tissues resulting from the nonuniform distribution of radiopharmaceuticals. Such investigations will be essential in the development of complication-probability biophysical models for nephrotoxicity in radiopharmaceutical therapy (8).

CONCLUSION

A computational multiregion model of a mouse kidney was developed and used to create a database of S values for 5 tissue regions and for a wide range of β- and α-emitters of interest in radiopharmaceutical therapy. The comprehensive set of regional S values facilitates preclinical internal radiation dosimetry of mouse kidney tissues and allows a more realistic estimation of the doses absorbed by different renal tissues from therapeutic radioligands with a nonuniform distribution in the kidneys, such as the ^{131}I-labeled sdAb investigated. The proposed model and the computed S values represent an improvement from the simplistic (less accurate) renal absorbed dose estimates assuming a uniform distribution of activity throughout the entire kidney. Such dosimetric improvement is expected to support preclinical nephrotoxicity studies essential for a better understanding and prediction of nephrotoxicity in humans.

KEY POINTS

QUESTION: How much does the nonuniform distribution of radionuclides used for radiopharmaceutical therapy impact the absorbed dose in mouse kidney tissues?

PERTINENT FINDINGS: A computational multiregion model of a mouse kidney was developed and was used to calculate S values for 5 kidney tissue regions for a wide range of β- and α-particle emitters of interest in radiopharmaceutical therapy. The database of regional S values indicates that consideration of a heterogeneous activity distribution in the kidneys can have a considerable impact on the absorbed dose estimates in specific renal substructures, particularly when dealing with α- and low- to medium-energy β-particle emitters.

IMPLICATIONS FOR PATIENT CARE: An improved dosimetry of therapeutic radiopharmaceuticals in mouse kidney tissues will contribute to a better understanding and prediction of nephrotoxicity in the presence of heterogeneous absorbed dose depositions in human kidneys.

REFERENCES

1. Flynn AA, Pedley RB, Green AJ, et al. The nonuniformity of antibody distribution in the kidney and its influence on dosimetry. *Radiat Res.* 2003;159:182–189.

2. Konijnenberg M, Melis M, Valkema R, Krenning E, de Jong M. Radiation dose distribution in human kidneys by octreotides in peptide receptor radionuclide therapy. *J Nucl Med.* 2007;48:134–142.

3. Bouchet LG, Bolch WE, Blanco HP, et al. MIRD pamphlet no. 19: absorbed fractions and radionuclide S values for six age-dependent multiregion models of the kidney. *J Nucl Med.* 2003;44:1113–1147.

4. Chigoho DM, Bridoux J, Hernot S. Reducing the renal retention of low- to moderate-molecular-weight radiopharmaceuticals. *Curr Opin Chem Biol.* 2021;63:219–228.

5. Svensson J, Mölne J, Forssell-Aronsson E, Konijnenberg M, Bernhardt P. Nephrotoxicity profiles and threshold dose values for [177Lu]-DOTATATE in nude mice. *Nucl Med Biol.* 2012;39:756–762.

6. Konijnenberg MW, Bijster M, Krenning EP, de Jong M. A stylized computational model of the rat for organ dosimetry in support of preclinical evaluations of PRRT with 90Y, 111In, or 177Lu. *J Nucl Med.* 2004;45:1260–1269.

7. Hobbs RF, Song H, Huso DL, Sundel MH, Sgouros G. A nephron-based model of the kidneys for macro-to-micro α-particle dosimetry. *Phys Med Biol.* 2012;57:4403–4424.

8. Wessels BW, Konijnenberg MW, Dale RG, et al. MIRD pamphlet no. 20: the effect of model assumptions on kidney dosimetry and response—implications for radionuclide therapy. *J Nucl Med.* 2008;49:1884–1899.

9. D'Huyvetter M, De Vos J, Caveliers V, et al. Phase I trial of 131I-GMIB-Anti-HER2-VHH1, a new promising candidate for HER2-targeted radionuclide therapy in breast cancer patients. *J Nucl Med.* 2021;62:1097–1105.

10. Eckerman K, Endo A. ICRP publication 107: nuclear decay data for dosimetric calculations. *Ann ICRP.* 2008;38:7–96.

11. D'Huyvetter M, De Vos J, Xavier C, et al. 131I-labeled anti-HER2 camelid sdAb as a theranostic tool in cancer treatment. *Clin Cancer Res.* 2017;23:6616–6628.

12. Vargas CS, Struelens L, D'Huyvetter M, Caveliers V, Covens P. Assessment of mouse-specific pharmacokinetics in kidneys based on 131I activity measurements using micro-SPECT. *EJNMMI Phys.* 2022;9:13.

13. Miller BW, Gregory SJ, Fuller ES, Barrett HH, Barber HB, Furenlid LR. The iQID camera: an ionizing-radiation quantum imaging detector. *Nucl Instrum Methods Phys Res A.* 2014;767:146–152.

14. Treuting PM, Kowalewska J. Urinary system. In: Treuting PM, Dintzis SM, eds. *Comparative Anatomy and Histology: A Mouse and Human Atlas.* Academic Press; 2012:229–251.

15. Barone R, Borson-Chazot F, Valkema R, et al. Patient-specific dosimetry in predicting renal toxicity with 90Y-DOTATOC: relevance of kidney volume and dose rate in finding a dose-effect relationship. *J Nucl Med.* 2005;46(suppl 1):99S–106S.

16. Kiess AP, Minn I, Vaidyanathan G, et al. (2*S*)-2-(3-(1-carboxy-5-(4-211At-astato-benzamido)pentyl)ureido)-pentanedioic acid for PSMA-targeted α-particle radiopharmaceutical therapy. *J Nucl Med.* 2016;57:1569–1575.

17. Bergsma H, Konijnenberg MW, van der Zwan WA, et al. Nephrotoxicity after PRRT with 177Lu-DOTA-octreotate. *Eur J Nucl Med Mol Imaging.* 2016;43:1802–1811.

18. Strigari L, Konijnenberg M, Chiesa C, et al. The evidence base for the use of internal dosimetry in the clinical practice of molecular radiotherapy. *Eur J Nucl Med Mol Imaging.* 2014;41:1976–1988.